Methods in Hydrothermal Single Crystal Growth of Synthetic Quartz

Undergraduate Thesis

Andrew J. Stewart - 972259050
University of Toronto 04/2000

Table of Contents

1 **Abstract**

2 **Introduction**

4 **Theory**

7 **Experimental Methods**
- 7 Furnace Design
- 9 Temperature Gradient
- 11 Autoclave Design
- 13 Seed Preparation
- 13 Growth Solutions
- 14 Experimental Procedure
- 16 Rose Quartz
- 16 SEM Analysis
- 16 Thin Sections

17 **Results**
- 22 Rose Quartz
- 22 Surface Textures
- 29 Thin Sections

31 **Discussion**

36 **Conclusions**

37 **Future Research Possibilities**

38 **Acknowledgments**

References

Appendix A – Calculation of Safe Internal Vessel Diameter
Appendix B - Sample fill amount calculation
Appendix C – pH Calculations
Appendix D – pOH determinations
Appendix E – Pure Water Composition
Appendix F – Copy of the Laboratory Manual

Abstract

Setup and experimental procedures for hydrothermal α-quartz crystal growth has been examined. Synthetic quartz is grown using a vessel subjected to a thermal gradient. Silica source material is dissolved into solution in the bottom, 400°C part of the vessel. The hot solution moves up in the vessel by convection to the cooler, 350°C top of the vessel which houses a seed crystal. Supersaturated solution at the seed crystal precipitates material onto the seed thereby growing the crystal. A furnace with three heating elements was designed and built to establish the thermal gradient necessary for quartz growth. Using this setup, growth of quartz crystals has been observed using distilled water and solutions of NaOH, Na_2CO_3, KOH and CsOH. Most runs were conducted over 5 days. Longer runs have also been performed, one producing a crystal of over 1cm in length. SEM imaging has been used on some of the grown crystals to examine the surface features revealing very well developed crystal facets as well as possible nucleation site features. Thin section analysis of grown crystals show no optical difference between the natural seed crystal material and the freshly grown material.

Introduction

Hydrothermal quartz growth has been used in the production of industrial synthetic quartz crystals since the late 1940s. The basic principles of growth are common for a variety of minerals and have been well developed. In general, a source material of SiO_2 (termed lasca) is dissolved into an aqueous solution and then precipitated onto an existing crystal face (of a seed crystal). To facilitate this process, higher temperatures are used to dissolve the lasca; then lower temperatures near the seed crystal cause solution supersaturation and precipitation onto the seed. An example of the ideal temperature gradient for optimal growth is provided in Figure 1A.

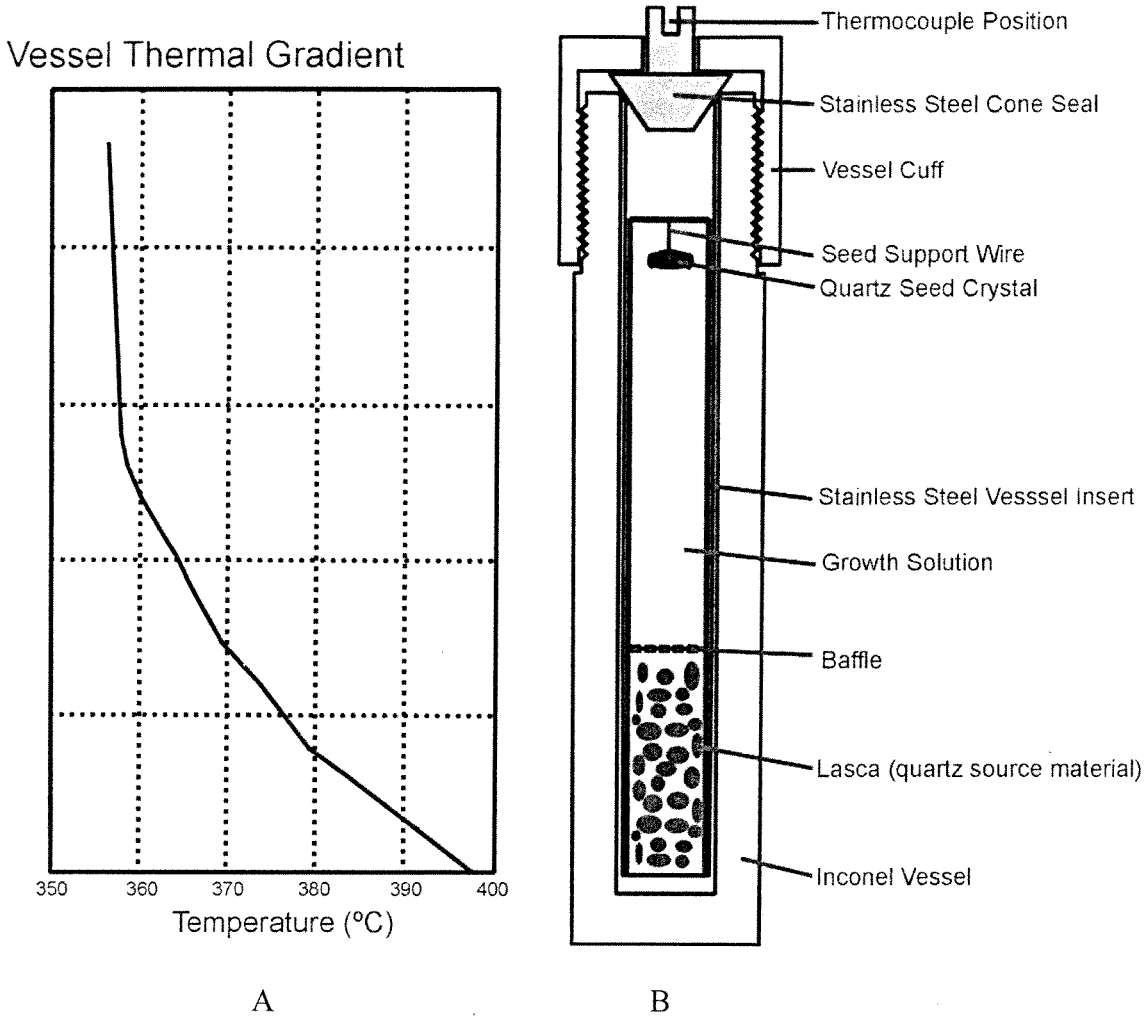

Figure 1 – A) optimal thermal gradient through the sample vessel; B) internal setup of the vessel contents; notice the higher temperature in the source area as compared with the almost isothermal area in the seed region.

Theory

The hydrothermal method of quartz crystal growth was pioneered early in the 20th century by Spieza (detailed in Wooster, 1946). The method exploits the changes in the solubility of silica with temperature and pressure. In aqueous mediums, silica dissolves by the mechanism:

[1] $SiO_{2\,(solid)} + 2\,H_2O \leftrightarrow H_4SiO_4\,(aq)$ (Dove and Rimstidt, 1994)

or $r SiO_{2\,(solid)} + nH_2O \leftrightarrow (SiO_2)_r \cdot nH_2O$ (Walther and Helgeson. 1977)

As the dissolved silica concentration increases, a silicon dimer may be formed by:

[2] $2\,H_4SiO_4\,(aq) \leftrightarrow H_6Si_2O_{7\,(aq)} + H_2O$ (Dove and Rimstidt, 1994)

In basic solutions, silica solubility is increased due to the formation of the SiO_3^{2-} aqueous species by the mechanism:

[3] $SiO_{2(Quartz)} + 2\,OH^- = SiO_3^{2-} + H_2O$ (Laudise and Kolb, 1969)

An increase in hydroxyl concentration shifts the equilibrium to the right, thereby dissolving more silica into solution with increasing pH. This increase in the silica solubility is additionally dependent on temperature and pressure.

At ambient temperature and pressures, the equilibrium of reaction [3] lies too far to the left to be functionally useful for any type of silica solubility related to crystal growth (Laudise, 1973). The solubility of SiO_2 is known to increase significantly with increased temperatures and pressure (Ibid.). However, in pure water, where reactions [1] and [2] control silica solubility, at higher temperature (400°C) and increased pressure (2 Kbar), solubility of silica is still less than 0.1 wt%; though still a greater then ten-fold increase to that at ambient conditions (Laudise and Kolb, 1969). Conversely in basic aqueous solutions (containing higher hydroxyl concentrations), reaction [3] becomes the dominant mechanism of silica solubility. The combination of increasing solubility with temperature and pressure with the increased solubility due to reaction [3] allows overall silica solubility to increase dramatically. Indeed, a 1.0 molar solution of NaOH increases the solubility to several weight percent at 400°C and 2 Kbar (Laudise and Kolb, 1969).

Now that we are able to dissolve significant amounts of silica into the solution, it must be transported and precipitated to form a crystal. A small α-quartz seed crystal is used on which the growth occurs. To facilitate precipitation, a state of supersaturation must be achieved in the vicinity of the seed crystal. The experiment is set-up such that the area in the vessel with the source material is hotter than the area with the seed crystal (normally above the source area) (see Figure 1A and B). The hotter temperature in the source area allows for increased solubility of the lasca (Figure 2A). The hotter saturated solution moves upwards in the vessel from the source area by convection (Ballman and Laudise, 1963) (see Figure 2B). As the saturated solution cools in the upper area, it becomes increasingly supersaturated. Lower activation energy associated with growth on a preexisting quartz surface versus a non-silicate surface (such as the side of a steel vessel) catalyses precipitation onto the seed and inhibits spurious nucleation on other surfaces (Figure 2C). Once the upper solution has cooled and precipitated some silica onto the seed, it is replaced by renewed saturated flux from below and sinks down in the vessel to warm again and dissolve more silica (Figure 2D). Thus the mechanism works essentially as a conveyor belt dissolving lasca and precipitating quartz onto the seed.

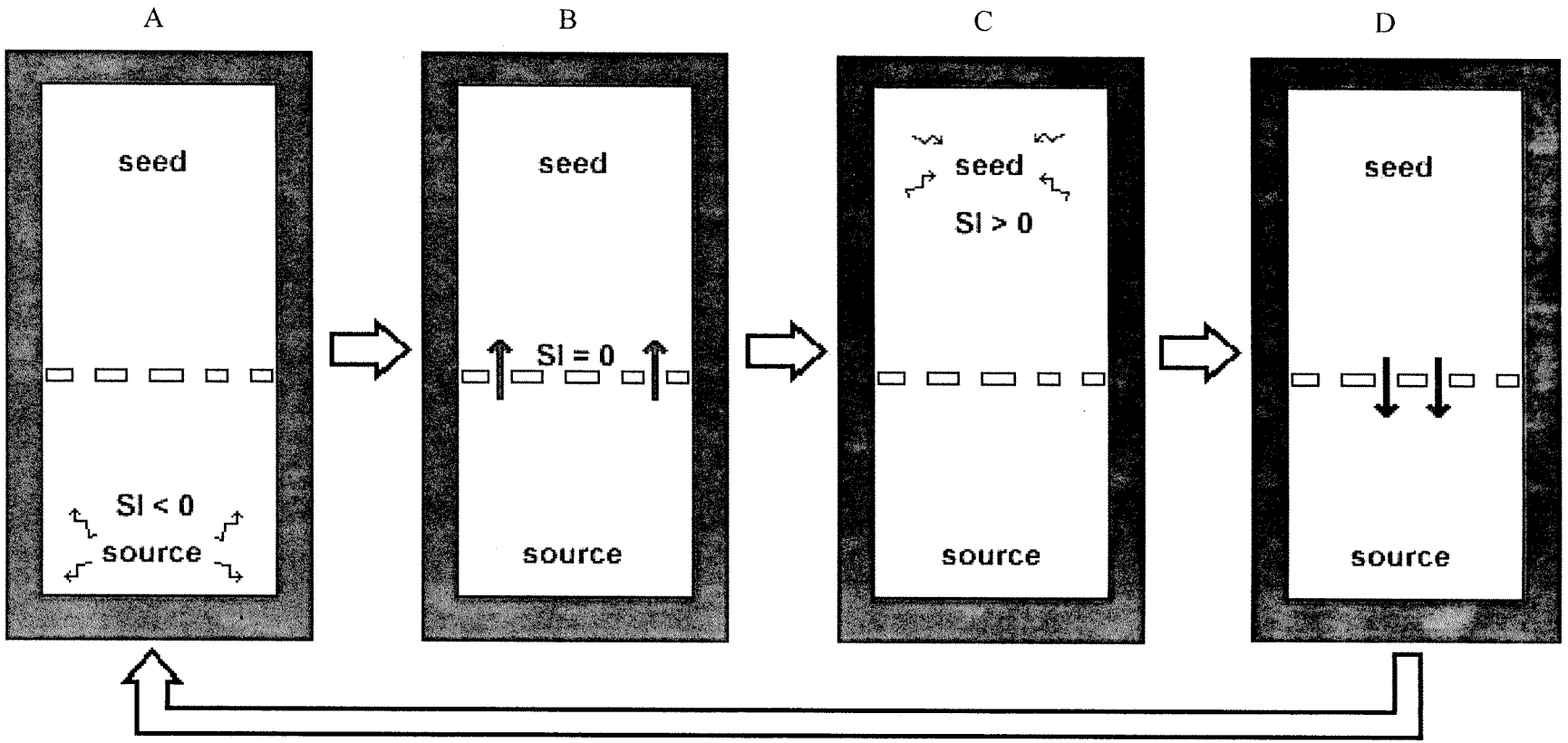

Figure 2 – Convection in the vessel: A) in the warmer source area, the solution is undersaturated (saturation index, SI < 0) resulting in dissolution of the silica source material; B) the warmer solution rises in the vessel due to convection; C) in the upper, cooler region, the solution is supersaturated (SI > 0) and comes out of solution onto the lowest energy surface, the quartz seed; D) the cooled, lower silica concentration part of the solution flows back downward in the veseel and the process begins again.

Experimental Methods

Furnace Design

Much of our initial work focussed on achieving an optimal temperature gradient for quartz growth. To customize a previously existing furnace for our purpose, ceramic insulation pieces were designed and fitted to maximize the amount of insulation around the vessel housing the sample. This insulation acts to reduce temperature fluctuations during experimental runs and maintain the integrity of the thermal gradient within the furnace. Slight modifications were also made to the furnace to allow an additional thermocouple to access the top of the sample vessel for more precise temperature control and safety during experiments. The final internal layout of the furnace can be seen in Figure 3.

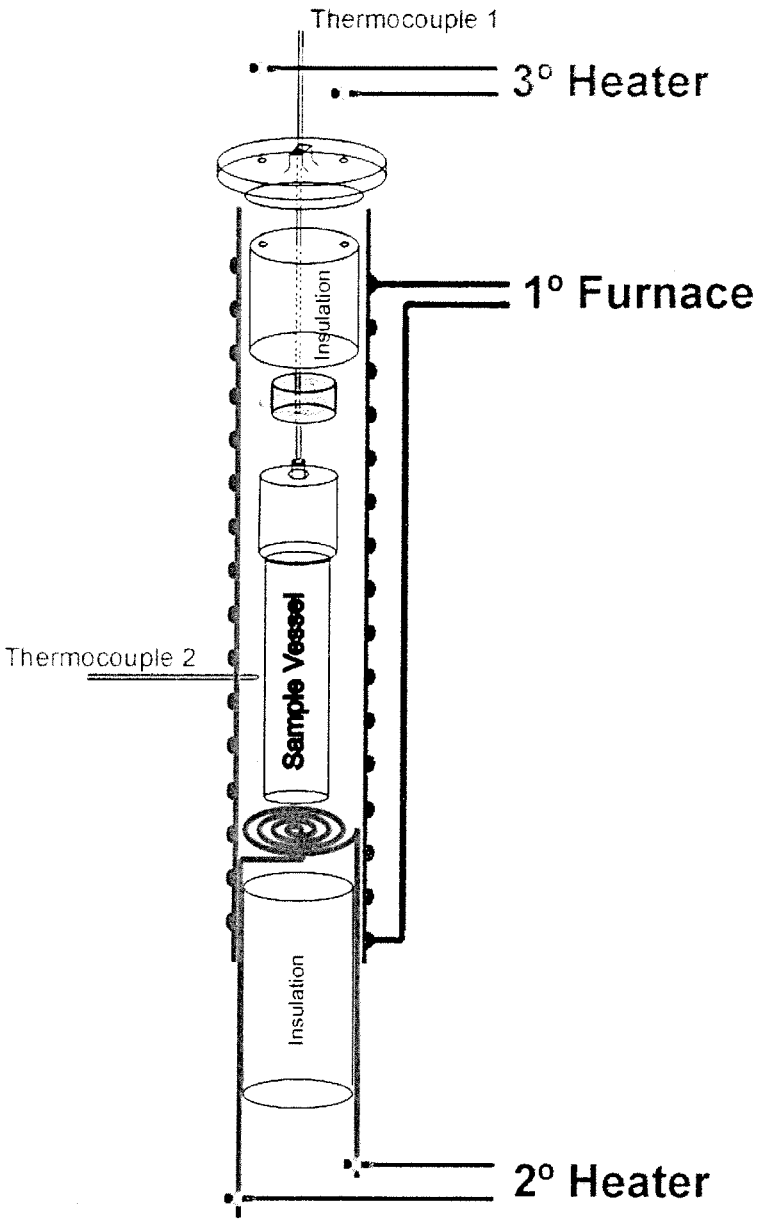

Figure 3 – Internal furnace layout and vessel position.

Temperature Gradient

Once the initial furnace modifications had been made, the furnace temperature characteristics were determined. Figure 4 displays the progression of temperature gradients as the furnace has been refined. The target optimal thermal gradient for hydrothermal quartz growth is given by the solid curve. The gradient in the basic, unmodified, single heater element furnace (only the "1° Furnace" in Figure 3) is clearly inadequate as it is completely opposite to the desired gradient (Figure 4: dashed-circle line vs. solid triangle line). As a first step in modifying the gradient, a new heater element was built and installed below the sample vessel area to perturb the curve to be hotter in the bottom source area. The result was a much improved gradient (Figure 4: dashed diamond line). However, while the bottom, source temperatures, are high enough to promote dissolution of the lasca, the volume within which stable growth can occur (i.e. a zone of near-zero temperature gradient) was still too small to reliably produce crystals of uniform grade. To create a longer isothermal growth zone, a third heater was designed for the top of the vessel to even out the temperature in the upper, growth area. The resulting gradient (Figure 4: dashed-square line) is quite close to the optimal conditions. This three element gradient allows ample area for source material to dissolve as well as a long isothermal zone (more than 10 cm) in which crystals may be grown. Again, the final furnace set-up and heater configuration can be seen in Figure 3.

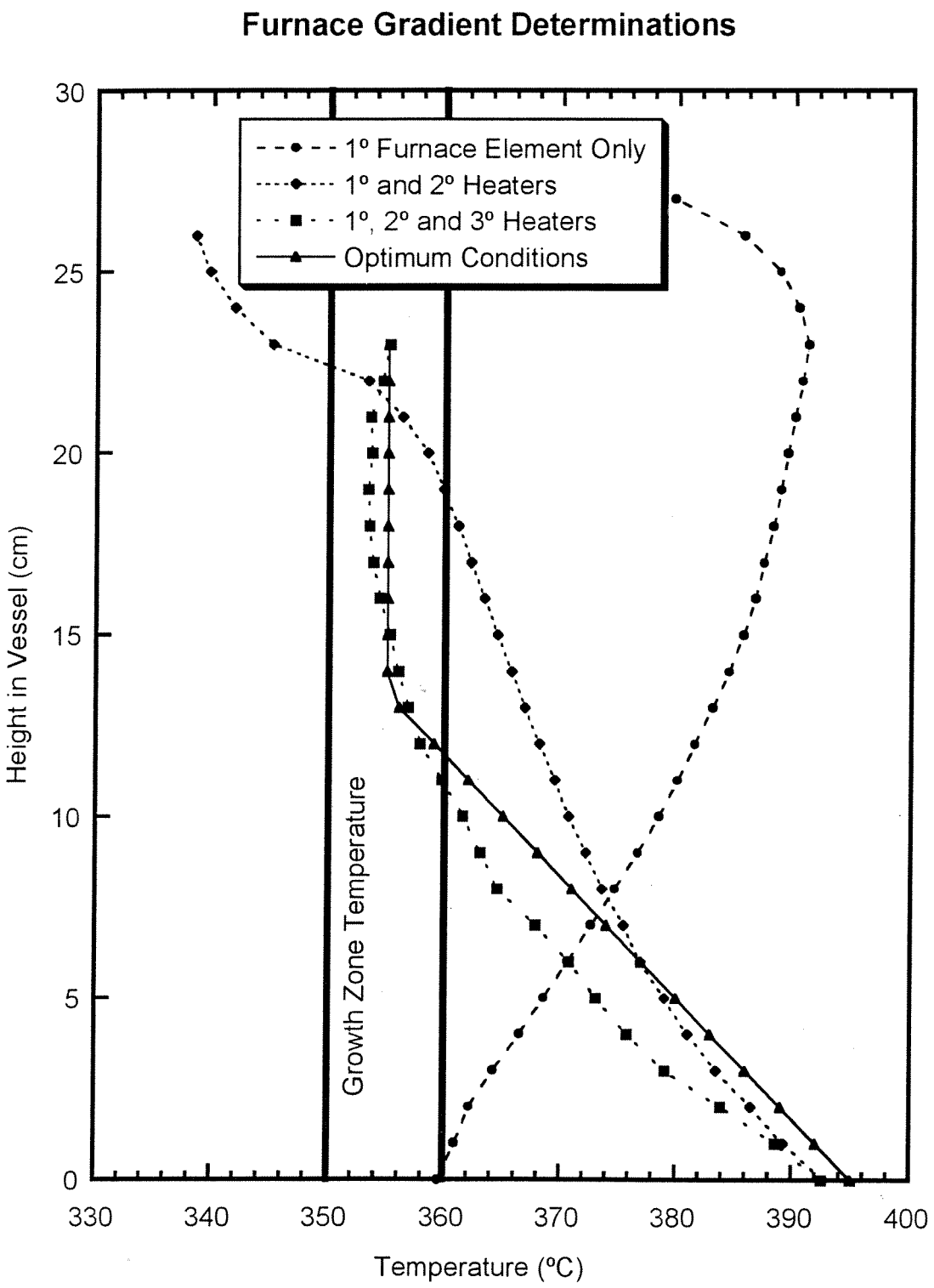

Figure 4 – Plot of temperature as a function of distance along the vessel axis showing the effects of furnace configuration on the concordance between the optimum thermal gradient and the measured gradient.

The temperature measurements made to determine the thermal gradient were done in situ, within a dry sample vessel (without vessel cuff or seal in place). It is expected that during actual runs, the temperature gradient is somewhat less dramatic due to the convective action of the solution evening out the temperature. However, it is likely that this in situ gradient determination process provides a much more reliable estimation of actual run thermal gradients compared with the values given in most of the literature which use external vessel temperatures to infer the internal gradient (for example: Laudise *et.* al, 1965; Buehler and Walker, 1974; Brown and Thomas, 1960).

For each of the three heating elements, completely separate Variac control systems were assembled. This allowed increased flexibility in adjusting the entire gradient as each element acts separately. Extensive dry experimentation was conducted to determine the best combination of settings for an optimal thermal gradient. Overnight testing using a temperature recorder indicated that there was very little fluctuation in temperature once an equilibrium state had been established. Therefore, overnight adjustments during production runs are unnecessary.

Autoclave Design

A modified sample vessel and cone seal was designed and constructed (detailed layout can be seen in Figure 5). The modifications were made to a large conventional cold-seal vessel (Figure 6). The new design has a wider bore, allowing for growth of larger crystals. Calculations were performed to determine the width to which the vessel could be bored out safely for use at the desired pressures (see Appendix A for detailed calculations). A stainless steel insert and seal were employed to help prevent corrosion of the pressure vessel by the growth solution. The seal has been designed to operate within the furnace at experimental temperature as opposed to outside the furnace as in standard cold-seal operation. Additionally, the seal is solid with no opening (unlike cold-seal operation), the vessel forms a closed system. Thus pressure within the vessel occurs when the system is raised in temperature and the aqueous solution expands to fill the void space and generate pressure.

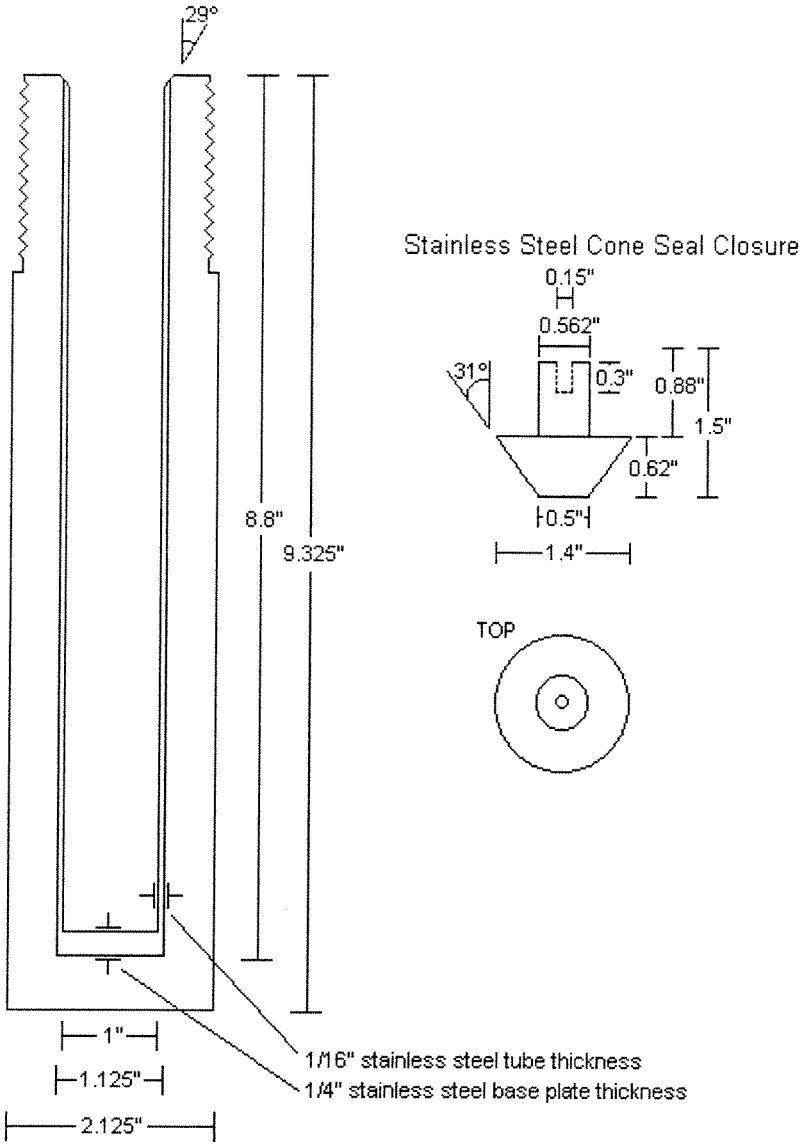

Figure 5 – Modified autoclave dimensions

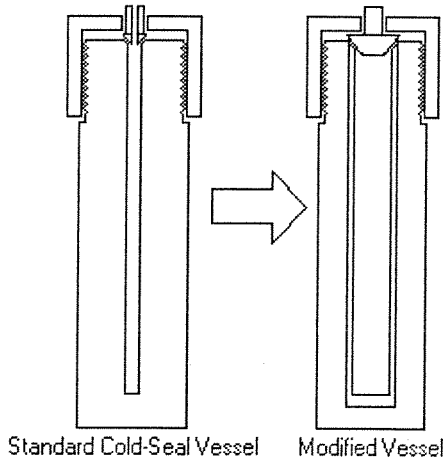

Figure 6 – Conversion of the Standard cold seal vessel to the growth vessel

Seed Preparation

α-Quartz crystal seeds used in our experiments were derived from natural euhedral crystals with good optical clarity. The seeds were cut perpendicular to the c-axis, forming so called "Z-cut" seeds (Brown and Thomas, 1960). Using this procedure, the prism faces {1100} were preserved in the seed, however there were no rhombohedral surfaces {1101} remaining. The cut surfaces can be defined as pseudo-faces (0001) and $(000\bar{1})$.

A method for seed suspension has been investigated to find a means by which a maximum surface area is available for growth while seed size is minimized. A clamping method has been utilized to hold the seed. This method has proved effective during growth runs and there were no instances of the seed falling from the support. Mounted on the seed support wire is a baffle that has been designed to help separate the hotter source region and the cooler growth zone. In this fashion the two areas will more closely approximate isothermal zones and the thermal change is localized across the baffle (Ballman and Laudise, 1963). The baffle will also help minimize contamination of the growth area by undissolved source material.

Growth Solutions

Five solutions were prepared for examination: Sodium Hydroxide (NaOH), Potassium Hydroxide (KOH), Cesium Hydroxide (CsOH), Sodium Carbonate (Na_2CO_3), and distilled water (H_2O). All solutions were prepared in 1.0 molal concentrations with University of Toronto Geology Department tap distilled water and high purity pelleted or powdered compound.

Experimental Procedure

Before beginning each experiment, a seed crystal was cut, weighed and measured for its dimensions. The seed was then fastened to a piece of platinum wire that clamps the crystal in place at three points. The clamped seed was hung from a larger support wire (seen in Figure 1).

A natural lasca supplied by Quartec has been used as the source material for all of our experiments. Before being placed into the vessel, lasca pieces were crushed using a steel mortar and pestle into sizes no more than 1.5 cm in diameter. About 30g of the crushed lasca was placed into the bottom of the vessel for each run. Above the lasca was placed a platinum perforated baffle. The seed was then suspended on a stainless steel wire which held the seed in position in the upper area of the vessel.

From the amount of lasca added, seed size and total vessel volume, the free volume within the vessel was calculated. Solution was added to the vessel to fill 73% of the void space, which at the temperature of the experiment, will expand to create an internal pressure of about 1.3kbar using the equation of state from Haar *et.* al (1984). A sample calculation is provided in Appendix B.

Once everything had been added to the vessel, the cone seal was set in position and the screw-on cap put on very tightly to hold the seal in place. Molykote was used on the vessel threads to help prevent thread binding. In later experiments (runs 14 and 15) Molykote was not used as it may have be responsible for previous thread seizing. No vessel thread seizing occurred when Molykote was not used. An entry and removal harness wire was attached and used to lower the prepared vessel down into the furnace. The thermocouples, tertiary (3°) heater and insulated top were then put into place on the furnace. Each heater element was then tested for continuity to detect the presence of any short circuits within the furnace.

The furnace was then slowly warmed up, mainly using the primary (1°) heater element. Once the vessel had reached 300°C, the power settings were lowered to predetermined values and the furnace slowly rises in temperature to establish a gradient in the vessel between 350°C and 400°C. The best equilibrium temperatures were established using settings of about 0.46 amperes (into the Variac) to the primary furnace, 8.5-9.0 volts from the secondary heater and 12.0-12.5 volts from the tertiary heater.

Most experiments were run for about 5 days (see Table 1 for exceptions). Over the duration of the run, the temperature was recorded and small power adjustments were made to ensure the proper temperature gradient was maintained. Once the run was complete, the power was turned off to all the heater elements and the vessel removed from the furnace and allowed to cool. The cooling vessel was examined for signs of leaking (such as a powdery residue). The cap and seal are taken off and the experimental products removed from the vessel and collected. The solution was examined for quantity of quartz precipitate, which can offer an indication of the solubility of the lasca during the run. The support wires and vessel were all examined for signs of spurious crystal growth and corrosion. As well, of course, the seed crystal was weighed and measured to determine any growth which may have occurred.

Rose Quartz

The synthesis of rose quartz was attempted following the methodologies outline in Hosaka *et.* al (1986). A quartz seed was grown using 1.0 molal NaOH in the presence of 1.00g of TiO_2. The grown crystal was then subjected to a heat treatment for 13 hours at 1200°C packed in a $CaCO_3$ charge containing 1% powdered hematite (Fe_2O_3). In theory iron should diffuse into the crystal forming intervalence charge transfer sites with Ti^{4+} which may have been taken up as an impurity during the growth process. The pink colour of natural rose quartz has been attributed to this charge transfer (Smith *et.* al, 1978), though other examinations suggest that the colouration is due to inclusions of the mineral dumortierite (Ma, 1997 and Applin and Hicks, 1987).

SEM Analysis

Scanning electron microscope work was done on a sample grown in each of the five solutions and an unused seed crystal (acting as a control for comparison). A JEOL JSM-840 scanning electron microscope was used and pictures were taken using either Polaroid Polapan 400 or Polaroid type 55 film. Before analysis, each of the sample crystals were cleaned using acetone and an ultrasonic cleaning device to remove organic and particulate matter. The samples were then mounted on 1cm SEM sample buttons and carbon coated. To ensure a good conductive contact between the crystal and the button, carbon paint was used to connect the lower edge of the samples to the button surface.

Thin Sections

Polished thin sections were made from the product crystal of runs 2 (NaOH), 3 (KOH), 8 (H_2O) and 11(Na_2CO_3). The crystals were cut parallel to the c-axis in a direction corresponding to a (1210) face. On the slide the section was mounted with the (1210) face upwards. The sections were examined using both a reflected light petrological microscope and a transmitted light petrological microscope. Digital microscopic images were taken using a video capture apparatus attached to a PC.

Results

We have conducted a series of five day experiments all at the same pressure and temperature, but containing different growth solutions. All experiments were performed using natural quartz seed crystals cut perpendicular to the c crystallographic axis. Most experiments resulted in measurable growth of synthetic quartz, although the absolute growth rate was found to be very much dependent on the nature of the growth solution (Table 1). The greatest amount of growth within the 5 day period occurred using 1 molal sodium carbonate, resulting in an increase in the thickness of the original seed crystal of 3.8 millimetres, corresponding to an average growth rate of about 0.75 mm/day (Run 6). Figure 7 is a photograph of the product from that experiment, and clearly shows the amount of growth with respect to the original seed (outlined in red dashed lines), and that the new quartz overgrowth was beginning to "engulf" its support hanger. The largest crystal grown to date is shown in Figure 8. This is the product of run 13, a 23 day run in Na_2CO_3. While the actual daily growth rate is less than that of run 6, due to the longer run (and wider seed crystal) the product is much bigger.

Slower growth rates were achieved with the other solutions (Table 1). pOH calculations were conducted to determine the affect of the different solutions on reaction [3] provided in the introduction. The calculations at experimental conditions are presented in Appendix D (pH calculations are presented in Appendix C). The pOH was calculated to be 5.3 for pure water; 0.0 for the hydroxide solutions (NaOH, KOH and CsOH) and –0.3 for the sodium carbonate solution.

Run #	Solution composition (1.0m)	Seed thickness before (mm)	Seed thickness after (mm)	Run Duration (days)	Change in seed thickness	Calculated linear growth rate (mm/day)	Crystal length after 30 days (mm)	Notes
1	NaOH	N/A	N/A	5	N/A	N/A	N/A	Crystal dissolved somewhat
2	NaOH	3.3	4.1	5	0.8	0.16	4.8	Visible Growth
3	KOH	1.7	2.3	5	0.6	0.12	3.6	Visible Growth
4	CsOH	0.38	N/A	5	N/A	N/A	N/A	Vessel Leaked - No Growth
5	H2O	1.04	1.42	5	0.38	0.076	2.28	Partial Leak, some growth
6	Na_2CO_3	1.16	4.97	5	3.81	0.76	22.9	Partial Leak, growth (**Fig. 7**)
7	NaOH	1.3	N/A	N/A	N/A	N/A	N/A	Partial Leak, seed destroyed during removal
8	H2O	1.04	1.13	4	0.09	0.0225	0.675	Partial Leak, some growth
9	Na_2CO_3	7.8	9	5	1.2	0.24	7.2	Oblique Cut Seed
10	NaOH	1.05	1.09	2	0.04	0.02	0.6	Leak-Test Run, temperatures were low for the entire run
11	Na_2CO_3	2.01	3.8	18	1.8	0.1	3	Long Run, leaked dry
12	CsOH	2.95	3.12	4	0.17	0.0425	1.275	Temperatures were low at end
13	Na_2CO_3	1.3	12.1	23	10.8	0.47	14.09	Visible Growth (**Fig. 8**)
14	NaOH + TiO_2	1.8	1.9	9	0.1	-	-	Vessel Leaked - No Growth, White powder on top of seed accounts for 0.1mm increase, NOT growth
15	NaOH + TiO_2	1.25	2.32	7	1.07	0.15	4.59	Colourless, also had white powder on top of the seed, growth only on the lower see surface

Table 1 – Summary of all experimental growth runs conducted.

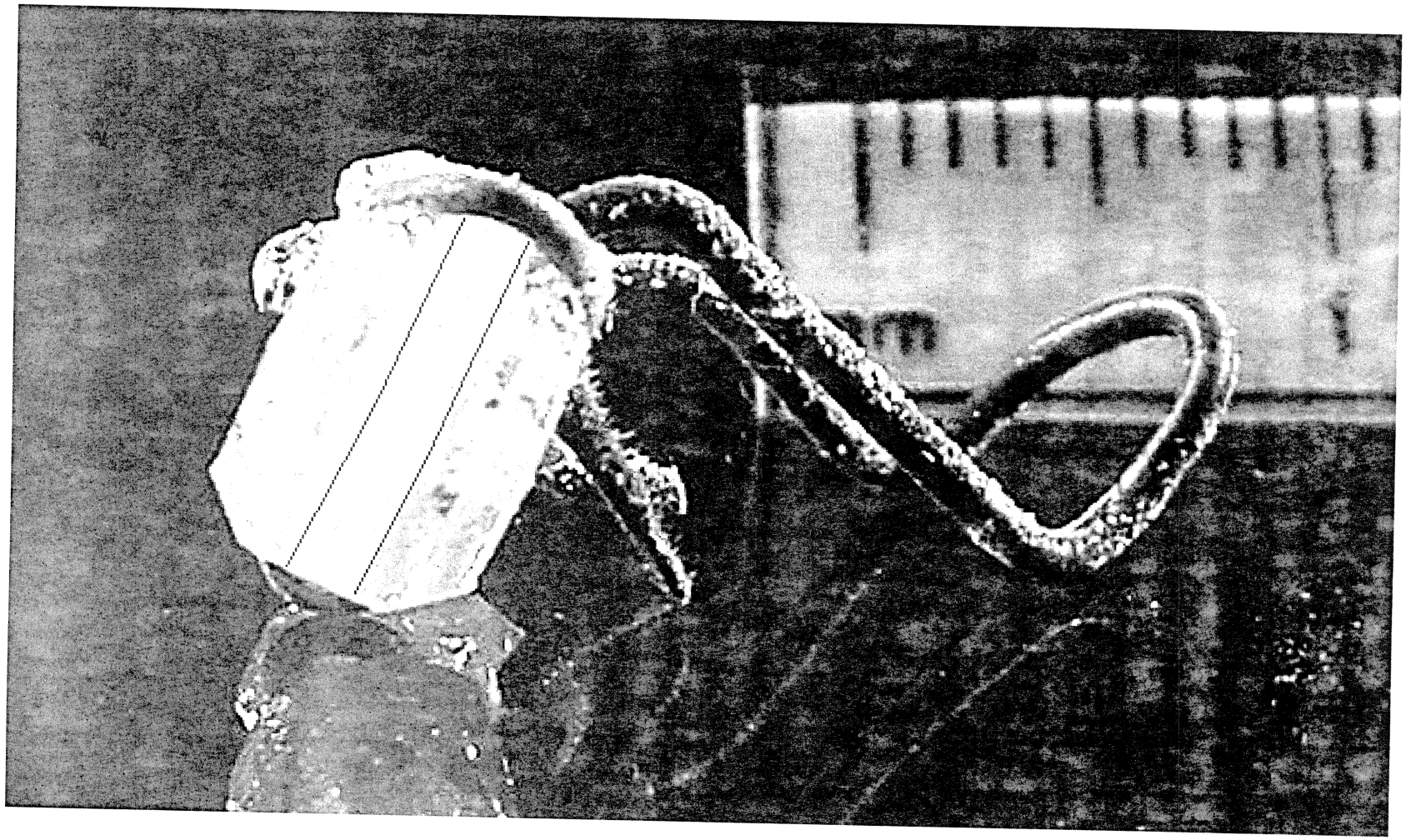

Figure 7 – Product of Run 6; grown in 1.0M Na_2CO_3 over 5 days (red lines indicate the location of the initial seed crystal).

Figure 8 –Product of Run 13; grown in 1.0M Na_2CO_3 over 23 days
(red lines indicate the location of the initial seed crystal).

From the summary Table 1, we can see that seal leaks have proved troublesome. It is suspected that the CsOH solution may have had a corrosive effect on the seal causing it to leak (Run 4). In an attempt to provide a better seal, the cone seal was re-machined and a copper spacer was added which would compress slightly to provide a positive pressure down on the cone seal following Run 4. Unfortunately, the copper appears to have deformed plastically from the pressure of the seal (i.e. the copper was not strong enough to withstand the pressure generated inside the vessel). Runs five through eight all had small leaks which appear to have sealed themselves with precipitated quartz, thereby allowing most of the solution to remain in the vessel. Due to the 'self-sealing' nature of these leaks, pressures were still generated in the vessel sufficient for growth on the seed crystal to occur. After run eight, the cone seal surface was re-machined and the deforming copper ring removed in a renewed attempt to create a good seal. However, some subsequent runs have still leaked for unknown reasons (runs 11 and 14).

One experiment has been conducted to examine the effect of different crystallographic orientation on growth (Run 9). The seed crystal was cut at an oblique angle to the {1101} rhombohedral faces, forming a face with the approximate crystallographic surface of (1211). In this experiment, it was observed that the crystal grew to form a smooth (1011) face on one half of the oblique cut while the other half was rough and had obviously not grown to form a face yet. Further examination is necessary to fully understand the nature of the oblique growth, however regardless of growth mechanism, the rate of growth on oblique cuts appears to be slow once a smooth face is established as compared with growth in the c-axis direction.

Rose Quartz

The growth of a seed crystal in the presence of TiO_2 was successful (run 15). A powder (assumed to be TiO_2) had accumulating on the top side of the seed crystal in the vessel assembly process. This accumulation prevented supersaturated solution from interacting with the top seed surface. Thus growth only occurred on the basal seed surface. After the heat treatment of the crystal, the seed was completely recrystallized and brittle. There was no sign of a pink colour. Near the platinum support wire, there was blue colouration and the surface appeared much smoother to that of the crystal away from the wire.

Surface Textures

The SEM provided valuable visual information about the growth crystals. The surface of the fast growing <0001> direction was examined on the samples. Figure 9 shows the surface of a seed prepared for use but not actually subjected to an experiment. This surface represents the initial topology of the seeds after they were cut using a diamond saw. The seed was not polished in any fashion following cutting (neither were the seeds before subjected to an experiment). Figure 10 is a picture of the surface of a crystal grown in Na_2CO_3. This sample has what appear to be many small spherical pits of differing relief (one of which is indicated by an arrow). Figure 11 is the surface of a CsOH grown crystal. The problems encountered at the end of this crystals growth are apparent in the figure. Deep, asymmetrical holes in the surface are present. An image to the same high magnification for a NaOH crystal can be seen in the inset image in Figure 12. From that image the very smooth surfaces can be seen, including the (0001) face. Finally, Figure 13 shows the high magnification surface structure of a crystal grown in distilled water. The surface has a globular texture much like that of so called "kidney ore" hematite.

The SEM also provided high resolution pictures of the facets grown on the crystals. The facets provide strong visual evidence of the growth which had occurred. Figure 12 shows a crystal with nicely formed {1101} faces around the edges of the crystal. A fissure across the surface also displays nice facets corresponding to the same crystallographic faces as the outer edges. In the inset, it can be seen how smooth these faces are even at very high magnification. Figures 14 and 15 again show the same well developed faces, this time in KOH and Na_2CO_3 grown crystals respectively. Figure 16, an image of a water-grown crystal, shows the faceting, however due to the globular texture of the water-grown samples, the faces and edges are not as well formed or separated as those grown with the addition of a mineralizer. For comparison with the faceted faces, I have included an image of the corner of the unaltered seed crystal (Figure 17). From this picture we can see there are definitely no rhombohedral faces {1101} present, and the edge between the prism faces and the (0001) face is rough and chipped. Unfortunately, due again to experimental problems, the Cesium hydroxide sample has become blurred due to late dissolution and thus no clear facets could be identified.

An additional SEM image can be seen in Figure 18. This is an image of the position of the support wire which had held the seed in the vessel. With the wire removed, its impression is left behind on the crystal.

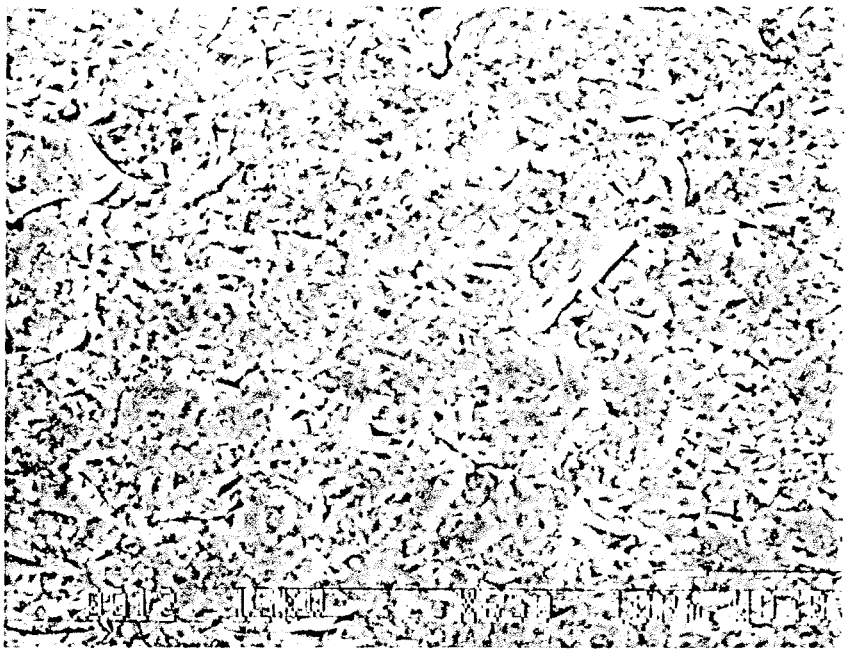

Figure 9 – (0001) surface of a ~~unused~~ untreated seed crystal

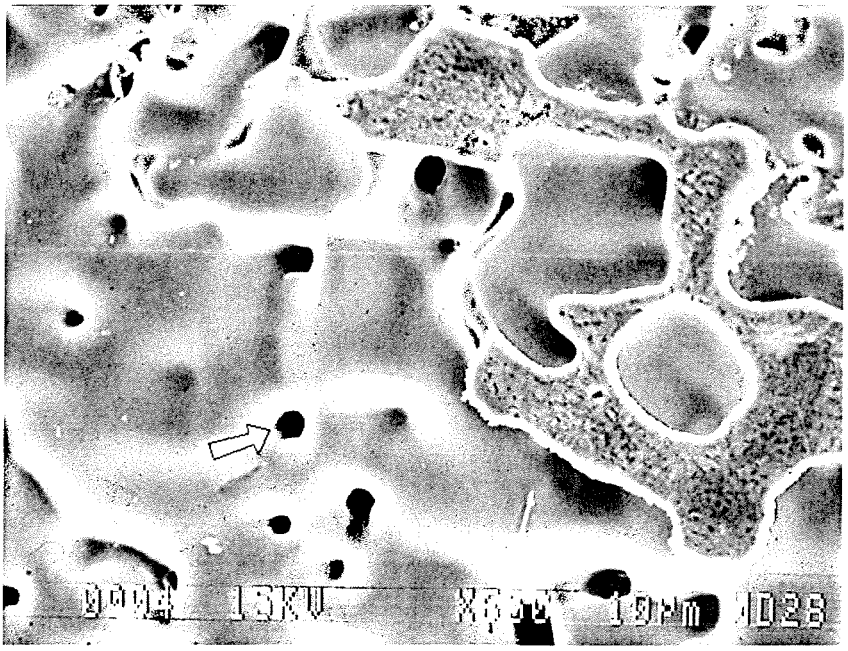

Figure 10 – (0001) surface of a crystal grown in Na_2CO_3

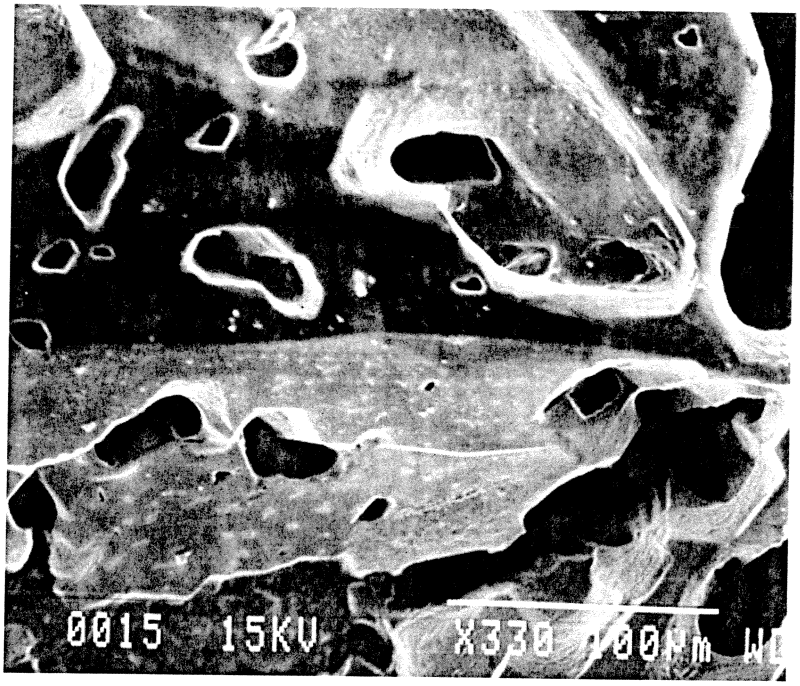

Figure 11 – (0001) surface of a crystal grown in CsOH

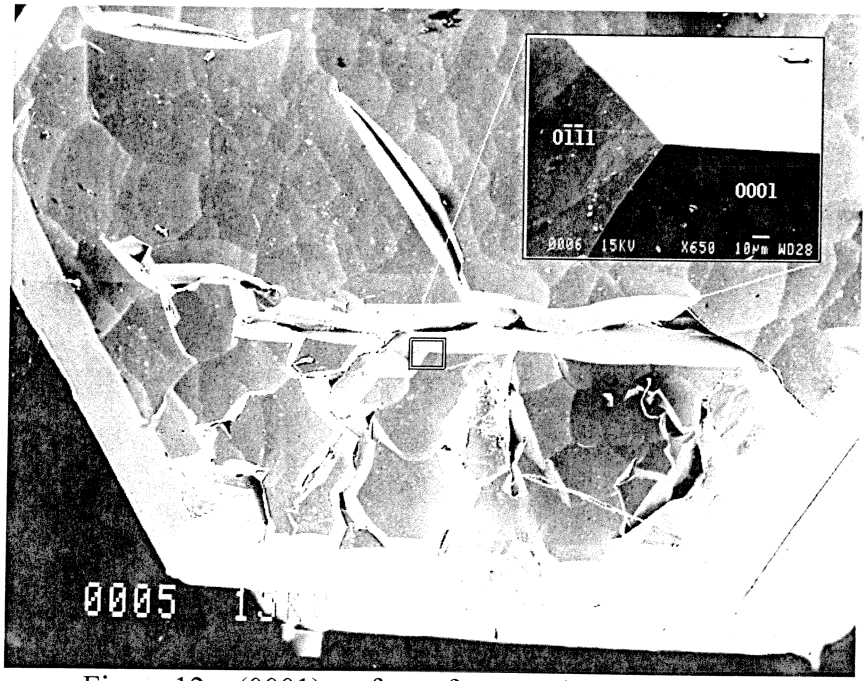

Figure 12 – (0001) surface of a crystal grown in NaOH

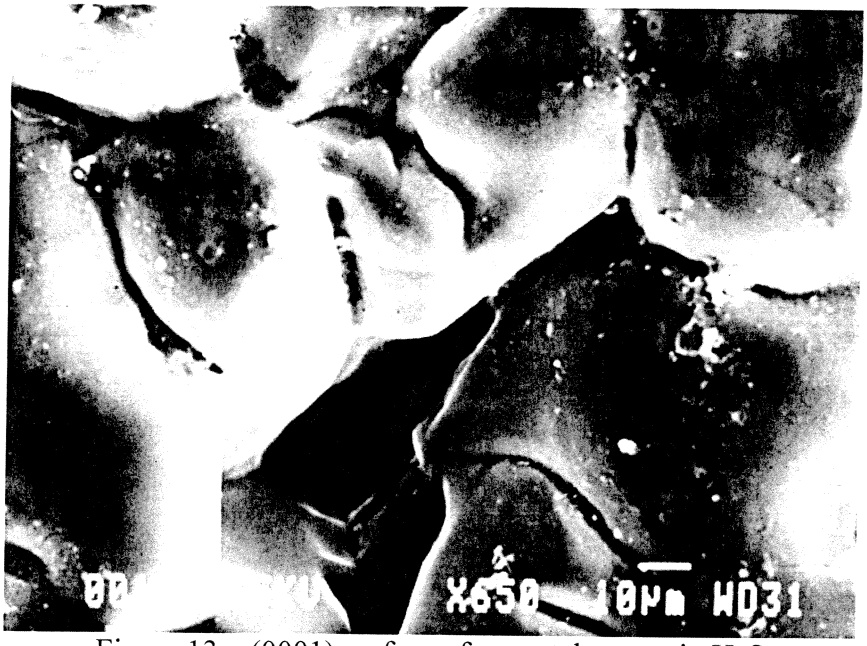

Figure 13 – (0001) surface of a crystal grown in H_2O

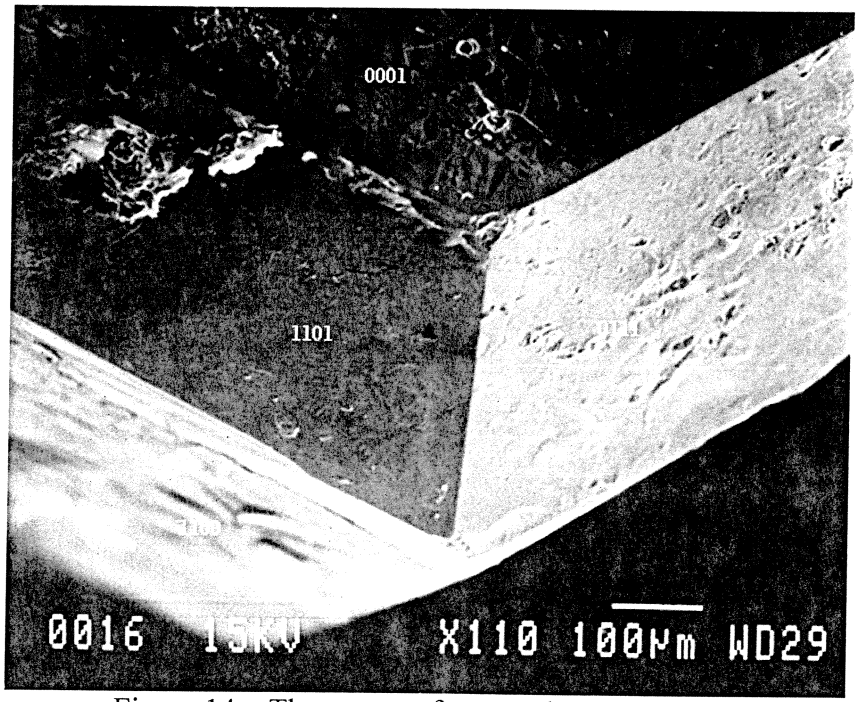

Figure 14 – The corner of a crystal grown in KOH

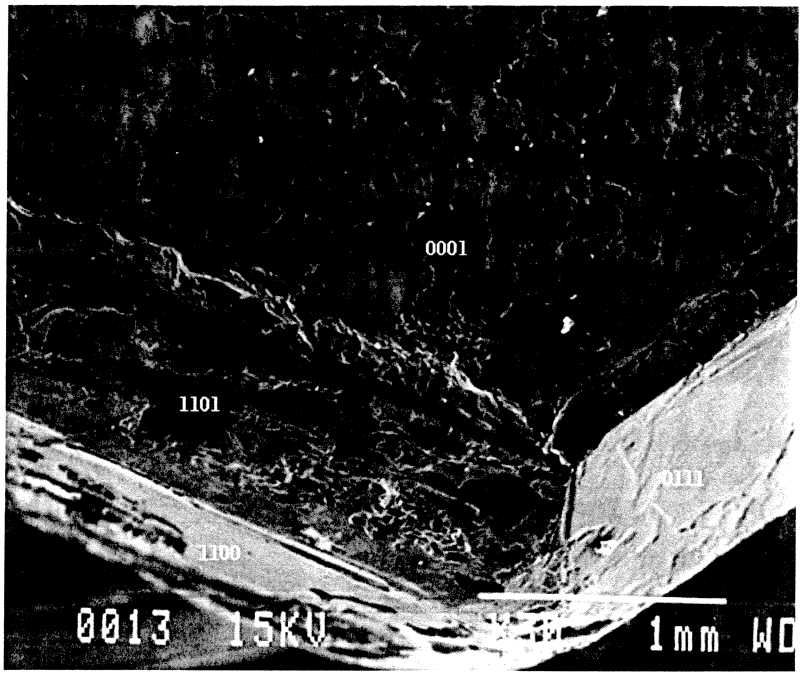

Figure 15 – The corner of a crystal grown in Na_2CO_3

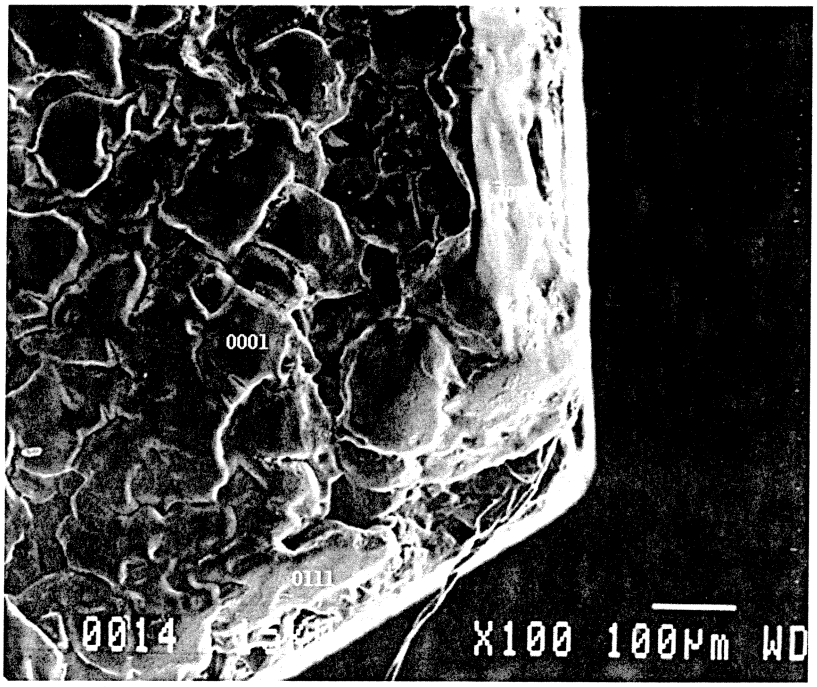

Figure 16 – The corner of a crystal grown in H_2O

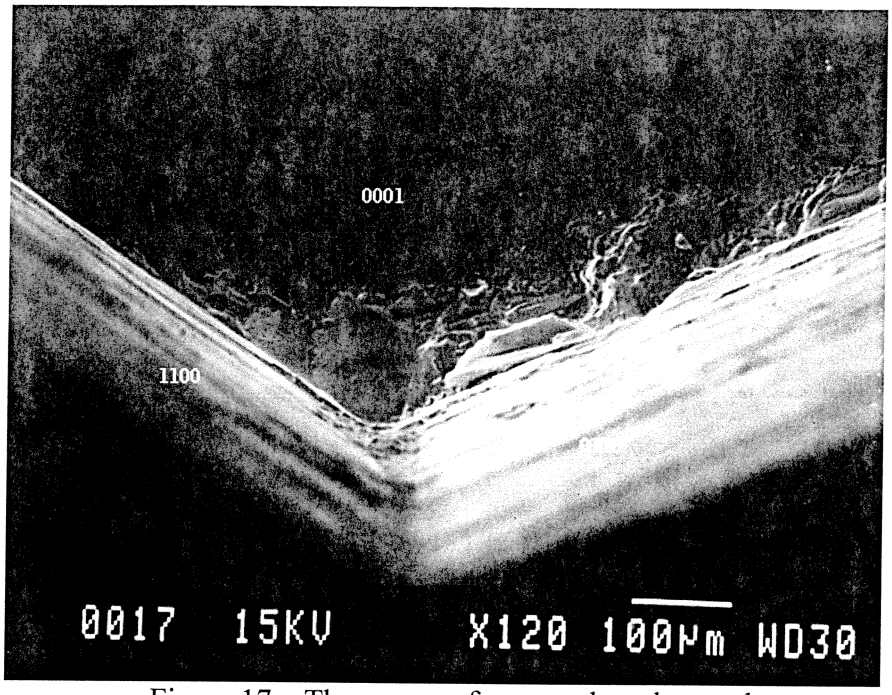

Figure 17 – The corner of a ~~unused~~ Untreated seed crystal

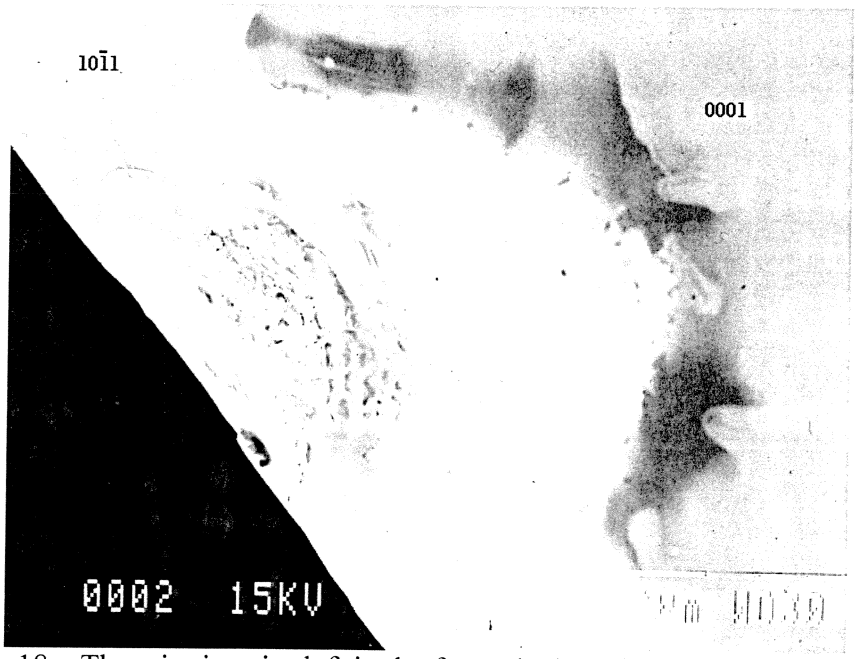

Figure 18 – The wire imprint left in the faceted edge of a crystal grown in KOH

Thin Sections

Of the four thin sections commissioned to be prepared, only samples from runs 2 (NaOH) and 3 (KOH) were useful for any type of analysis. The sections of runs 8 (H_2O) and 11 (Na_2CO_3) were destroyed in the preparation process and the resulting small fragmented pieces of the crystal are impossible to relate to the original crystal. Only one corner of sample 3 persisted intact. From this corner, the nice facet could be identified and thus the position of the new growth compared to that of the original seed crystal. The two areas are indistinguishable by optical examination and there were no inclusion anomalies in the area of intersection. The appearance of sample 2 is uniform as well and is presented in Figures 19 and 20. These two images also show the consistency of colouration and extinction between both the original seed crystal and the growth area (delineated by the red line). Please not that the slightly dark trace on Figure 19, which approximates the initial growth surface, is not a crystal structure, but a artifact from the slide making process. This streak continues into the epoxy beyond the margin of the crystal.

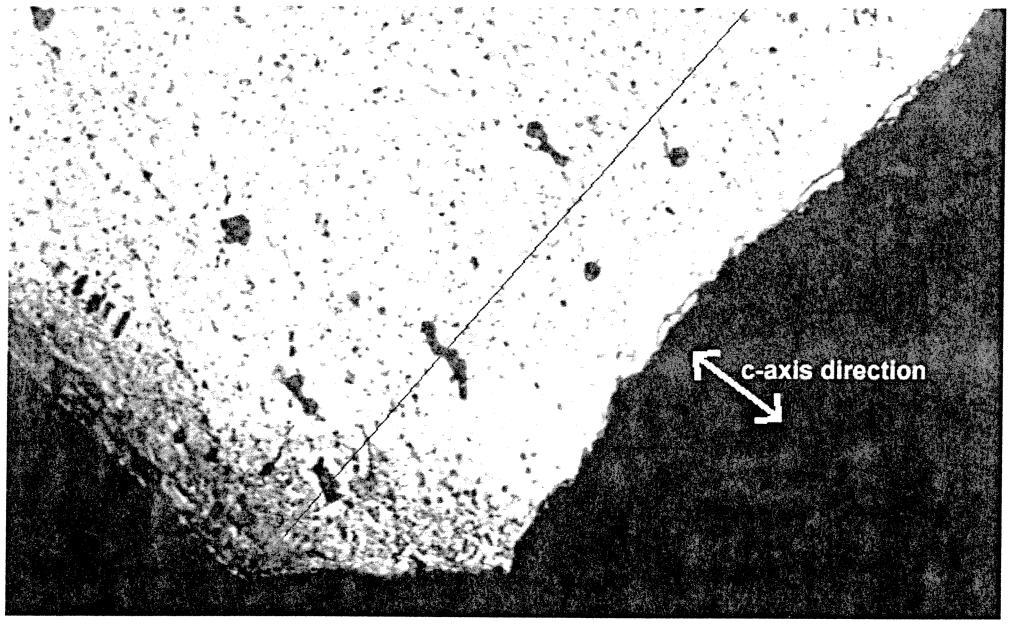

Figure 19 – The transmission of light through a quartz seed crystal (grown in 1.0M NaOH) cut parallel to the c-axis. The seed is oriented with the c-axis at an oblique angle to the polarised light. The red line indicates the boundary between the original seed (top left) and the freshly grown quartz (bottom right).

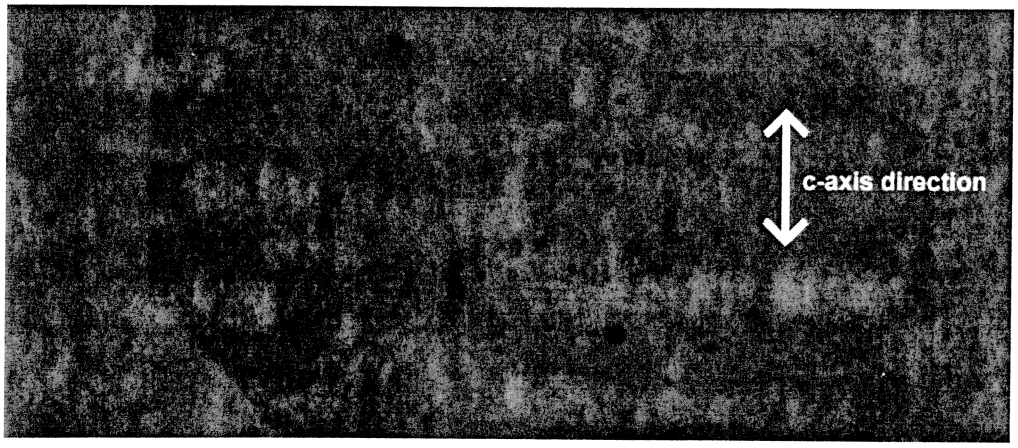

Figure 20 – The uniform extinction of the same quartz crystal in Figure 19 now oriented with c-axis parallel to the polarized light. The red line again indicates the boundary between the original seed (left) and the newly grown material (right).

Discussion

The furnace design and implementation as well as experimental procedure has been proved to be successful for the growth of synthetic α-quartz crystals. We have achieved growth rates up to 0.76mm/day. This growth rate reasonably consistent with those achieved by previous researches (Table 2). From this table, the cumulative relationship between solution concentration and pressure can be observed. The Yamashita study produced crystal with growth rates almost twice as fast as those formed by the methods described in this paper. The major significant difference is the pressure of the experiment. Brown and Thomas provide a demonstration of how solution composition is also a significant factor in the growth rate.

Growth Rate (mm/day)	Solution	Temperature (°C)	Pressure (Kbar)	Author
1.7	1.0M NaOH	345-390	1.6	Wood and Ballman, 1966
1.4	1.0M Na_2CO_3	350-400	1.55	Yamashita, 1975
0.76	**1.0M Na_2CO_3**	**355-400**	**1.3**	**Current Study**
0.55	0.83M Na_2CO_3	360-400	1.6	Brown and Thomas, 1960

Table 2 – Comparison of selected previous growth experiments and the current study.

Through our 5 day experiments, we have successfully grown crystals using all solutions examined: distilled water, NaOH, Na_2CO_3, KOH and CsOH. The most successful run to date was using Na_2CO_3. It is expected that these differences are caused by two factors. Firstly, reaction [3] proceeds to dissolve more silica into solution with increasing hydroxyl concentration. With this in mind, the pOH of each solution was calculated (Appendix D). To achieve this, the K_w of water at our experimental conditions of temperature and pressure was calculated using the computer program SUPCRT (results are included in Appendix C).

From the pOH results we can see that there is an increasing hydroxyl concentration from H_2O < XOH < Na_2CO_3. From our experimental observations, the rates of growth match this trend with maximum rates achieved as H_2O (0.076mm/day) < XOH (0.16mm/day) < Na_2CO_3 (0.76mm/day).

The second factor believed to be involved in these results is an effect of sodium in the solution. It has been well established that silica solubility increases with NaCl content of a solution, at least at pressures above 400bars (Von Damm *et.* al, 1991 and Fournier, 1983). This increased solubility is due to changes in water structure to allow increased hydrogen bonding (Dove and Rimstidt, 1994). The increased hydrogen bonding leads to an increase in the stability of $H_4SiO_{4\,(aq)}$, the hydrated species produced by reaction [1] (Ibid.). Thus it is probable to expect this effect (or at least a similar, lesser effect) may also occur in other sodium solutions. Hence with increased sodium concentration, reaction [1] is driven to the right, increasing silica solubility. This theory is supported by the results presented here. 1.0M Na_2CO_3 solution leads to 2.0M Na^+ concentration into the solution, whereas 1.0M NaOH provides only 1.0M Na^+. The other solutions provide no sodium. Our observations of growth rate Na_2CO_3 >> NaOH >> KOH, CsOH, H_2O is consistent with such a mechanism.

While most runs in Table 1 are self explanatory, runs 11 and 12 are worth a bit more in depth discussion. Run 11 was our first attempt at a longer duration growth period, 18 days. While a significant amount of growth was measured (1.8mm), it was somewhat of a disappointment especially in comparison to the 3.8mm grown over 5 days in run 6. The vessel had leaked dry in the longer run. Obviously however, there was a time period over which the vessel solution was convecting and acting to grow the seed crystal. Thus the vessel either suffered from a slow progressive leak which eventually dried out the solution or else there was a sudden catastrophic release of the fluid. It may be possible to determine which mechanism was responsible by microscopic analysis or x-ray darkening of the crystal. We would expect a slow leak would produce a pattern of slower and slower growth features in the crystal (smaller layers) and a quick leak to leave a more uniform crystal.

Run 12, as can be seen in the SEM image (Figure 11) underwent dissolution. From the record of the experimental temperatures it can be seen that high temperatures were observed (~ 15° above desired) early in the process, leading to growth. However in an attempt to correct the high temperatures, the furnace was lowered to a temperature about 20° below desired, after which the experiment was halted. Since the crystal dimensions indicate growth had occurred, yet dissolution features are also present, the crystal did grow initially, but then must have stopped growing then began to dissolve. The adjustments made to the furnace temperature were mostly made to the 2°, bottom heater. Thus the low temperatures recorded by the top and side thermocouples relate to a very low bottom (source) temperature. From the recorded temperature, the top of the vessel was 20° cool and the side thermocouple 23° cool. Therefore, the temperature at the bottom must have been even farther off because that is the source of the cooled vessel temperature. The result of this is likely a reversal of the temperature gradient within the vessel; the top, seed region having a temperature of approximately 330°C and the bottom, source area having a temperature likely under 200°C. This would prevent silica from dissolving in the source region, thereby inhibiting supersaturation in the vicinity of the seed by the convection model (Figure 2). The seed would begin to act as the hotter source area by dissolving in the warmer solution and sinking in the vessel due to it's higher density, then precipitating in the cooler source region. Hence the conveyor belt would be reversed. This mechanism and the temperature are obviously not as efficient as the reverse, normal conditions, but it would lead to dissolution of the seed and thus is consistent with the observations of the temperature change and seed condition.

In regard to the obliquely cut seed crystal, it is difficult to make reliable conclusions from a single sample. However, it appears that since the (1101) face was formed on the oblique cut, but not the adjoining (0111) face, it is likely that the original cut was not precisely along (1211), but closer to the (1101) face. Since the growth of crystals is most rapid when not occurring on faces (since face planes have the highest atomic density, thus require more atoms to form), rapid growth occurred on the oblique cut until a face developed. Because the cut was more closely approximating the (1101) face, it was the first to form along the cut, whereupon growth slowed significantly due to

the high atomic concentration of the face. Growth of the oblique cut had not proceeded far enough to begin to form the (0111) face.

The rose quartz growth attempt was not very informative as no rose quartz was made. The recrystallization which occurred is due to the polymorph change from α-quartz to tridymite (the stable quartz structure at low pressure and 867-1470°C) with β-quartz occurring between the two polymorphs from 573 and 867°C (Deer *et.* at, 1992). Since the single seed was recrystallized to many smaller grains, it became brittle. The blue colouration and smooth texture is likely the result of a small amount of carbonate melt having occurred in the vicinity of the platinum wires. The colour being attributed to some unknown silica-calcium-iron (and possibly, though unlikely, platinum) mineral phase. The smooth surface of the areas is due to the rapid cooling of the liquid to form some glass.

From the SEM images, it can be seen that all samples were altered from the unused seed crystal surface. This indicates that either growth or dissolution has occurred. From the measurements of the seeds before and after runs, as well as the strong support of the well faceted SEM images (for all but the CsOH sample, which would be expected to grow proper facets if grown without problem), we can confidently say growth had occurred with all solutions.

In the higher magnification images of the growth surface, we can attempt to infer growth mechanisms. The Na_2CO_3 sample has what appear to be small round pits (Figure 10). These pits may be the boundaries between different nucleation sites on the seed crystal. The nucleation sites would have grown both outward (in the c-direction) and to the sides (towards the prism faces). This type of growth would produce domes of silica on the surface. Where two nucleation domes meet there should be a furrow and where more than two meet (at a triple point for example), a ovoid pit would be expected. In Figure 10 we can see what may be interpreted as furrows running between some of the pits. Depending on the number of nucleation sites and hence their density on the surface, the proximity of the furrows and pits would differ. Many nucleation sites would produce

a more even surface with very close, shallow furrows and pits. If very few nucleation sites are present, deeper furrows and pits should be observed as well as larger nucleation domes.

From the higher magnification (650x) images (Figures 10, 12 inset and 13) we can see that the sample grown in water (Figure 13) has a very 'globby' texture of domes. Thus we would expect that in water less nucleation sites occur on the growing surface. The globular surface is better seen in the lower magnification image of this crystal, Figure 16. The inset in Figure 12 shows how very smooth the surfaces are on the crystal formed in NaOH solution. Thus we would expect that there were very many nucleation sites on this crystal leading to the smooth surface we see (such shallow furrows that they cannot be readily seen). Finally the Na_2CO_3 grown crystal in Figure 10 seems to display a condition intermediate between the other two. The effect of the number of nucleation sites on the growing surface is not precisely known. It would be expected however that the more nucleation sites on a face, the faster it would grow because more growth is taking place at more places.

From the thin sections we can observe that there is optical homogeny between the grown quartz and the original natural quartz seeds on which it has grown. As well, there is not a line of inclusions following the initial growth surface as may have been expected. This indicates that the growth onto the surface occurred without significant error and followed the cut seed surface precisely, at least for the crystals growth with NaOH and KOH.

Conclusions

The methods described in this paper outline a successful procedure for the hydrothermal synthesis of α-quartz crystals optically identical to natural α-quartz. Repeated growth experiments have been performed, however the reliability of growth is still not complete. Growth has been achieved using five solutions: distilled water, NaOH, Na_2CO_3, KOH and CsOH. Of these solutions, the fastest crystal growth has been achieved using Na_2CO_3.

Future Research Possibilities

While it has been established that increased pressure enhances silica solubility, the precise relationship between the pressure and its effect on the growth of a quartz seed is not known. Further examinations of growth with pressures in excess of 1.3kbar are important to ensure that the most efficient possible growth process is found.

In addition to examinations of the effects of higher pressures, solution concentration should be studied as well. While reaction [3] is obviously driven to the right with increased hydroxyl concentration, and previous studies have shown a dramatic growth rate increase with solution molality (see Table 1), it is unknown whether the solubility of quartz increases exponentially with molality right up to the saturation point of the base.

The three heater element furnace configuration developed for this project is very flexible and could be used for some interesting crystal growth examinations. For example, with this set-up, the temperature gradient within the vessel may be modified over the duration of an experiment. Such an examination could involve growth cycles of hotter and cooler seed conditions, source conditions or both.

Due to the desired end-use of large production quartz crystal for electronics; the exact properties of a high quality quartz crystal for electronic applications must be examined. These desired qualities must be examined in relationship to the conditions of growth to ensure a viable final product.

Acknowledgments

I would like to thank James Brenan for all his help in showing me how to work just about everything I have used, all his advice on the direction of the project and his comments on previous drafts of this manuscript. Jim Mungall has also been friendly enough to provide me with sodium carbonate powder for my solutions and other materials as well as a last minute proofread of an early report. As well, thanks to Greg Anderson for his advice on aqueous speciation determinations and computer programs to help out. Finally I would also like to thank Karyn Gorra for all the pictures she has taken of my crystals.

References

Applin, K.R. and B.D. Hicks, (1987) Fibers of Dumortierite in Quartz. Am. Mineralogist. 72, 170-172.

Arnold, G.W. Jr., (1960) Defects in Natural and Synthetic Quartz. J. Phys. Chem. Solids. 13, 306-320.

Ballman, A.A., (1961) The Growth and Properties of Colored Quartz. Am. Mineralogist. 46, 439-446.

Ballman, A.A. and R.A. Laudise, (1963) Hydrothermal Growth. In: The Art and Science of Growing Crystals, J.J. Gilman (ed.). John Wiley & Sons, New York. 231-251.

Buehler, E. and A.C. Walker, (1949) Growing Quartz Crystals. The Scientific Monthly. LXIX, 148-155

Brown, C.S. and L.A. Thomas, (1960) The Effect of Impurities on the Growth of Synthetic Quartz. J. Phys. Chem. of Solids. 13, 337-343.

Deer, W.A., R.A. Howie and J. Zussman, (1992) The Rock Forming Minerals. Adison Wesler Longman, Essex, England.

Dove, P.M. and J.D. Rimstidt, (1994) Chapter 8: Silica-Water Interactions. *In* Heaney, P.J., C.T. Prewitt and G.V. Gibbs (eds.), (1994) Silica: Physical Behavior, Geochemistry, and Materials Applications. Mineralogical Society of America, Reviews in Mineralogy Volume 29. Washington, D.C.

Fournier, R.O., (1983) A Method of Calculating Quartz Solubilities in Aqueous Sodium Chloride Solutions. Geochimica et Cosmochimica Acta. 47, 579-586.

Haar, L., J.S. Gallagher, and G.S. Kell, (1984) NBS/NRC Steam Tables: Thermodynamic and Transport Properties and Computer Programs for Vapor and Liquid States of Water in SI Units. McGraw Hill, Montreal.

Hosaka, M. and S. Taki, (1981) Hydrothermal Growth of Quartz Crystals in NaCl Solution. J. of Crystal Growth. 52, 837-842.

Hosaka, M., T. Miyata, Y. Shimizu and O. Okuyama, (1986) Synthesis of Rose-Quartz Crystal. J. of Crystal Growth. 78, 561-562.

Joshi, M.S. and A.S. Vagh, (1964) Growth Spirals on Prism Faces of Cultured Quartz. Am. Mineralogist. 49, 1771-1773.

Kohman, G.T., (1963) Precipitation of Crystals from Solution. In: The Art and Science of Growing Crystals, J.J. Gilman (ed.). John Wiley & Sons, New York. 152-162.

Laudise, R.A., A.A. Ballman, and J.C. King, (1965) Impurity Content of Synthetic Quartz and its Effect upon Mechanical Q. J. of Phys. and Chem. of Solids. 26 (8), 1305-1308.

Laudise, R.A., E.D. Kolb, and J.P. DeNeufville, (1965) Hydrothermal Solubility and Growth of Sphalerite. Am. Mineralogist. 50,382-391.

Laudise R.A. and E.D. Kolb, (1969) Hydrothermal Synthesis of Single Crystals. Endeavour. 28 (105), 114-117.

Laudise, R.A., (1973) Hydrothermal Growth. In: Crystal Growth: An Introduction, by P. Hartman. North-Holland Publ. 162-197.

Ma, C., (1997) Fibers in Rose Quartz: HRTEM & AEM Investigations. Geological Society of America, Abstracts. 29(6), 459.

Nakayama, F.S., (1971) Thermodynamic Functions for the Dissociation of $NaHCO_3^0$, $NaCO_3^-$, H_2CO_2 and HCO_3^-. J. Inorg. Nucl. Chem. 33, 1287-1291

Ohtomo, A., (1982) Growth of Synthetic Quartz and Its Trend. J. of Electronic Engineering. 19 (187), 34-38.

Van Praagh, G., (1947) Synthetic Quartz Crystals. Geological Magazine. 84 (2), 98-100.

Von Damm, K.L., J.L. Bischoff and R.J. Rosenbauer, (1991) Quartz Solubility in Hydrothermal Seawater: An Experimental Study and Equation Describing Quartz Solubility for up to 0.5M NaCl Solutions. Am. J. of Science. 291, 977-1007.

Walther, J.V. and H.C. Helgeson, (1977) Calculations of the Thermodynamic Properties of Aqueous Silica and the Solubility of Quartz and its Polymorphs at High Pressures and Temperatures. Am. J. of Science. 277, 1315-1351.

Wood, D.L. and A.A Ballman, (1966) Blue Synthetic Quartz. Am. Mineralogist. 51, 216-220.

Wooster, N. and W.A. Wooster, (1946) Preparation of Synthetic Quartz. Nature. 157, 297.

Yamashita, A., A. Shinomiya, and H. Kumasaki, (1975) Content Correlation of Fe and Alkali Metals in Synthetic Quartz. J. of Crystal Growth. 30, 27-28

Appendix B - Sample fill amount calculation

Raw data:

27.08g Lasca
Density of quartzite = 2.65 g/cm^3
$V_{vessel} = 98ml = 98cm^3$
$V_{support\ wire} = 0.8ml = 0.7cm^3$
$V_{seed} = 0.7ml = 0.6\ cm^3$
Fill = 73%

Calculations:

27.08g lasca ÷ 2.65 $g/cm^3 = 10.22cm^3$

$V_{available} = 98cm^3 - (0.7cm^3 + 0.6cm^3 + 10.22cm^3)$
$= 86.48cm^3$

$V_{solution} = 0.73 \times 86.48cm^3$
$= 63.1cm^3$
$= 63.1ml$

Therefore, 63.1ml of growth solution is added to the vessel.

Appendix C (page 2)

XOH (NaOH, KOH, CsOH)

$$XOH \leftrightarrow X^{+} + OH^{-} \qquad [C2]$$

Assumptions

All solutes are completely soluble in water (very large K_{eq})
All solutions were prepared in 1.0 Molal concentrations

350°C, 1300bar

$\log K_w = -10.501$
thus $K_w = 1 \times 10^{-10.501}$

Since the protons and hydroxyl ions in equilibrium with water must equal and there is an addition of 1.0M of OH^-, the expression for the hydroxyl concentrations can be rewritten as:

$$[OH^-] = [H^+] + 1.0M$$

Thus:

$$K_w = [H^+][OH^-] = [H^+]([H^+] + 1.0M) \approx [H^+](1.0M) = [H^+]$$

Since $[H^+] << 1.0M$

And:

$$1 \times 10^{-10.501} = [H^+]$$

Taking negative logarithms:

$$-\log[H^+] = 10.501$$

So, pH = 10.5

400°C, 1300bar

$\log K_w = -10.599$
thus $K_w = 1 \times 10^{-10.599}$

$$[OH^-] = [H^+] + 1.0M$$

$$K_w = [H^+][OH^-] = [H^+]([H^+] + 1.0M) \approx [H^+](1.0M) = [H^+]$$

Since $[H^+] << 1.0M$

$1 \times 10^{-10.501} = [H^+]$

Taking negative logarithms:

$-\log[H^+] = 10.599$

So, pH = 10.6

Na_2CO_3

$$Na_2CO_3 \leftrightarrow 2Na^+ + CO_3^{2-} \qquad [C3]$$

This reaction is obviously pH independent as there is no H^+ or OH^- contained in the reaction.

However;

$$CO_3^{2-} + H^+ \leftrightarrow HCO_3^- \qquad [C4]$$

$$HCO_3^- + H^+ \leftrightarrow H_2CO_3 \qquad [C5]$$

$$H_2CO_3 \leftrightarrow H_2O + CO_{2(g)} \qquad [C6]$$

Reaction [C6] only occurs in systems with a gas phase. Since this system is closed and contains no vapour phase at experimental conditions, this reaction can be ignored.

Assumptions

Na_2CO_3 is completely soluble in water (very large K_{eq})

Constants Calculations (derived from Nakayama, 1971)

$HCO_3^- = H^+ + CO_3^{2-}$

$$\log K_{HCO3-} = -3029.3/T + 7.1945 - 2.470 \times 10^{-2} \cdot T$$

350°C (623.15K)

$$\log K_{HCO3-,350°} = -3029.3/(623.15) + 7.1945 - 2.470 \times 10^{-2} \cdot (623.15)$$
$$= -4.86 + 7.1945 - 15.392$$
$$= -13.057$$
$$pK_{HCO3-,350°} = 13.057$$

$$K_{HCO3-,350°} = 10^{-13.057}$$

Appendix C (page 4)

400°C (673.15K)

$\log K_{HCO3-,400^\circ} = -3029.3/(673.15) + 7.1945 - 2.470 \times 10^{-2} \cdot (673.15)$

$= -4.5 + 7.1945 - 15.391$

$= -12.697$

$pK_{HCO3-,400^\circ} = 12.697$

$K_{HCO3-,400^\circ} = 10^{-12.697}$

$\mathbf{H_2CO_3 = H^+ + HCO_3^-}$

$\log K_{H2CO3} = -2914.16/T + 11.4685 - 2.700 \times 10^{-2} \cdot T$

350°C (623.15K)

$\log K_{H2CO3,350^\circ} = -2914.16/(623.15) + 11.4685 - 2.700 \times 10^{-2} \cdot (623.15)$

$= -4.676 + 11.4685 - 16.825$

$= -10.033$

$pK_{H2CO3,350^\circ} = 10.033$

$K_{H2CO3,350^\circ} = 10^{-10.033}$

400°C (673.15K)

$\log K_{H2CO3,400^\circ} = -2914.16/(673.15) + 11.4685 - 2.700 \times 10^{-2} \cdot (673.15)$

$= -4.329 + 11.4685 - 18.175$

$= -11.036$

$pK_{H2CO3,400^\circ} = 11.036$

$K_{H2CO3,400^\circ} = 10^{-11.036}$

pH Calculations

350°C, 1300bar

$\mathbf{HCO_3^- = H^+ + CO_3^{2-}}$

$K_{HCO3-,350^\circ} = 10^{-13.057}$

Thus:

$$10^{-13.057} = \frac{\{H^+\}\{CO_3^{2-}\}}{\{HCO_3^-\}}$$

Assuming infinite dilution:

$$10^{-13.057} = \frac{[H^+][CO_3^{2-}]}{[HCO_3^-]}$$

Appendix C (page 5)

Since K is very small, the reaction proceeds very strongly to the left (removing protons from the system). Starting with 1.0M CO_3^{2-}, 1.0M of hydroxyl ions will be formed from water as protons are used up and water continues to dissociate. As CO_3^{2-} is depleted and HCO_3^- becomes more common, the second reactions begins to remove protons as well:

$$\mathbf{H_2CO_3 = H^+ + HCO_3^-}$$

$$K_{H2CO3,350^\circ} = 10^{-10.033}$$

Thus:

$$10^{-10.033} = \frac{\{H^+\}\{HCO_3^-\}}{\{H_2CO_3\}}$$

Again, assuming infinite dilution:

$$10^{-10.033} = \frac{[H^+][HCO_3^-]}{[H_2CO_3]}$$

This reaction, like the other, has an equilibrium which strongly lies towards the left. Thus another mole of hydroxyl ions are released by this second reaction, resulting in a net concentration of OH^- of 2.0M per 1.0M CO_3^{2-}.

Thus:

$$K_w = [H^+][OH^-] \approx [H^+](2.0M) = 2[H^+]$$

And:

$$1 \times 10^{-10.501} = 2[H^+]$$
$$[H^+] = 1.58 \times 10^{-11}$$

Taking negative logarithms:

$$-\log[H^+] = 10.8$$

So, pH = 10.8

Appendix C (page 6)

400°, 1300bar

The equilibrium constants for the carbonate system between 350° and 400° are not significantly different. Thus I will not repeat all the calculations included with the 350°C determination for 1.0M Na_2CO_3 (above). Thus the reactions would both proceed essentially to completion to produce 2.0M OH^-.

$$K_w = [H^+][OH^-] \approx [H^+](2.0M) = 2[H^+]$$

$$1 \times 10^{-10.599} = 2[H^+]$$
$$[H^+] = 1.259 \times 10^{-11}$$

Taking negative logarithms:

$$-\log[H^+] = 10.9$$

So, pH = 10.9

Appendix D – pOH determinations

H_2O

350°C, 1300bar

$\log K_w = -10.501$

thus $K_w = 1 \times 10^{-10.501}$

$1 \times 10^{-10.501} = [OH^-]^2$

Taking negative logarithms:

$-2\log[OH^-] = 10.501$

$-\log [OH^-] = 5.25$

So, pOH = 5.25

400°C, 1300bar:

$\log K_w = -10.599$

thus $K_w = 1 \times 10^{-10.599}$

$1 \times 10^{-10.599} = [OH^-]^2$

Taking negative logarithms:

$-2\log[OH^-] = 10.599$

$-\log [OH^-] = 5.3$

So, pOH = 5.3

XOH (NaOH, KOH, CsOH)

pOH is temperature independent as $[OH^-]$ can be assumed to be independent of K_w as $[OH^-]_{solute} >> [OH^-]_{water\ derived}$.

Thus:

$[OH^-] = \sim 1.0M$

$-\log[OH^-] = 0$

And so:

pOH = 0

Appendix D (page 2)

Na_2CO_3

Similar to XOH, pOH is temperature independent as $[OH^-]$ can be assumed to be independent of K_w as $[OH^-]_{solute\ induced} >> [OH^-]_{normal\ water\ dissociation}$.

$[OH^-] = \sim 2.0M$
$-\log[OH^-] = -0.3$

Thus $pOH = -0.3$

Appendix E – Pure Water Composition

350°C, 1300bar

$\log K_w = -10.501$

thus $K_w = 1 \times 10^{-10.501}$

$$[OH^-] = [H^+]$$

Thus:

$K_w = [H^+][OH^-] = [H^+]^2$

$[H^+]^2 = 1 \times 10^{-10.501}$

$[H^+] = 5.62 \times 10^{-6}$M

400°C, 1300bar:

$\log K_w = -10.599$

thus $K_w = 1 \times 10^{-10.599}$

$$[OH^-] = [H^+]$$

Thus:

$K_w = [H^+][OH^-] = [H^+]^2$

$[H^+]^2 = 1 \times 10^{-10.599}$

$[H^+] = 5.02 \times 10^{-6}$M